Carbohydrate Polymers 83 (2011) 697–704

Contents lists available at ScienceDirect

Carbohydrate Polymers

journal homepage: www.elsevier.com/locate/carbpol

Fixed-bed column studies on the removal of copper using chitosan immobilized on bentonite

Cybelle Morales Futalan[a], Chi-Chuan Kan[b], Maria Lourdes Dalida[c], Chelo Pascua[d], Meng-Wei Wan[b,*]

[a] Department of Environmental Engineering, University of Philippines-Diliman, Quezon City 1800, Philippines
[b] Department of Environmental Engineering and Science, Chia Nan University of Pharmacy and Science, Tainan 71710, Taiwan
[c] Department of Chemical Engineering, University of Philippines-Diliman, Quezon City 1800, Philippines
[d] National Institute of Geological Sciences, University of Philippines-Diliman, Quezon City 1800, Philippines

ARTICLE INFO

Article history:
Received 11 May 2010
Received in revised form 26 June 2010
Accepted 17 August 2010
Available online 24 August 2010

Keywords:
BDST model
Breakthrough curve
Chitosan
Mass transfer zone
Thomas model

ABSTRACT

The use of chitosan immobilized on bentonite (CHB) in the removal of Cu(II) from aqueous solutions was investigated using a column system. The effect on the time of breakthrough and uptake capacity of the column was examined. The dynamics of the adsorption process were evaluated by using bed depth service time (BDST) model and Thomas model. The adsorption capacity of 14.92 mg Cu(II)/g CHB with 24 h breakthrough was achieved at 500 mg/L of initial concentration, bed height of 4.3 cm, and flow rate of 0.20 mL/min. The time of breakthrough decreases while breakthrough curves become sharper with increase in flow rate and influent concentration, and a decrease in bed height of the adsorbent. Moreover, Thomas model was an acceptable kinetic model. The BDST model was utilized to compute dynamic bed capacity (N_0), adsorption rate constant (k_{ads}), and critical bed depth (Z_0) at 29.94 g/L, 0.000857 L/(mg h) and 0.9187 cm respectively.

1. Introduction

Copper in waste effluents is generated by several anthropogenic sources such as electroplating industry, wire drawing, copper polishing and mining activities. It is one of the trace elements that are considered to be an essential nutrient required by the human body. However, ingestion at high dosages can lead to health problems such as lesions in the central nervous system, and liver and kidney damage, or Wilson's disease (Han et al., 2009). It is therefore important to remove excess copper in industrial effluents before discharging it into surface water and groundwater for the protection of human health and the environment.

There are several existing technologies in removing heavy metals like copper such as ion exchange, membrane separation, reverse osmosis, and chemical precipitation. These methods have several disadvantages such as being costly, ineffective in removing trace amounts of heavy metals, and generation of polluted by-products (Han et al., 2009; Popuri, Vijaya, Boddu, & Abburi, 2009). Among the physicochemical treatments, adsorption is an attractive method because it is easy to operate and is highly effective in removing heavy metals from effluents either with high solute loadings or dilute concentrations (Popuri et al., 2009). However, the utilization of commercialized adsorbents like activated carbon is expensive, which leads to high operational costs (Tor, Danaoglu, Arslan, & Cengeloglu, 2009). Research on low-cost, natural adsorbents such as montmorillonite, agricultural wastes and seafood processing wastes has been recently gaining ground due to its availability, short operational time, and non-generation of sludge. Previous studies include banana pith, sea weed, hazel nut shell, maize leaf, pillared Fe-montmorillonite, and chitosan (Li & Wu, 2010; Popuri et al., 2009; Qaiser, Saleemi, & Umar, 2009).

For heavy metal's contaminations in groundwater, applying permeable reactive barrier (PRB) for the recovery of metals is a practical environmental remediation technology by building filters containing environmental friendly adsorbent. Among the natural adsorbents, chitosan has been reported to illustrate the highest metal chelating capacity (Varma, Deshpande, & Kennedy, 2004). It is an attractive, functional biopolymer due to its remarkable properties such as biodegradability and non-toxicity (Machado, Lopes, Sousa, & Airoldi, 2009). However, using pure chitosan as an adsorbent has several disadvantages such as low surface area, low specific gravity, high cost, and weak chemical and mechanical properties (Chang & Juang, 2004). Moreover, it easily dissolves in acidic solutions and tends to form a hydrogel in aqueous media, which results in the inaccessibility of its binding sites. Therefore, chitosan is modified either chemically or physically to improve its strength for practical applications.

* Corresponding author. Tel.: +886 6 266 0615; fax: +886 6 213 1291.
E-mail addresses: peterwan@mail.chna.edu.tw, wann612@yahoo.com (M.-W. Wan).

0144-8617/$ – see front matter © 2010 Elsevier Ltd. All rights reserved.
doi:10.1016/j.carbpol.2010.08.043

Chemical modification such as crosslinking or chitosan derivatives based on carboxymethyl and hydroxamic acid is costly and/or has complicated preparative methods (Chang & Juang, 2004; Wan, Kan, Rogel, & Dalida, 2010). Physical modification provides an immobilization material for chitosan that will result in the easy access of its binding sites, and would reduce the quantity of chitosan used to synthesize the composite adsorbent material (Wan et al., 2010). Clay materials are made up of hydrous aluminosilicates sheets. These materials are considered as low-cost adsorbents for heavy metal removal. However, complex surface modifications on clay materials are needed such as pillaring to improve their adsorption capacity in removing Cu(II), Co(II), and Cd(II) (Li & Wu, 2010; Wu et al., 2009). Bentonite, a type of clay material, has a high specific surface area and is mechanically and chemically stable (Bhattacharyya & Gupta, 2006). Using a simple process in the immobilization of chitosan on bentonite particles would result in lower production costs and improved mechanical and chemical stability (Wang & Wang, 2008).

There are numerous batch studies performed on the removal of heavy metals using pure chitosan or its derivatives, with only a few studies reported on the packed bed column system. However, only column studies could provide readily available support for direct applications in the PRB remediation of contaminated groundwater.

The purpose of the study is to investigate the performance of chitosan immobilized on bentonite (CHB) in the removal of Cu(II) from aqueous solutions in a fixed-bed system. The effect of influent concentration, bed height, and flow rate on the column performance and shape of the breakthrough curves was evaluated. Kinetic column models namely bed depth service time (BDST) model and Thomas model were applied to describe the dynamic performance of the adsorption process and assist in predicting the breakthrough curves.

2. Materials and methods

2.1. Chemicals

All the chemicals utilized in the present study were of analytical grade. Chitosan, low molecular weight, with 75–85% degree of deacetylation, was obtained from Sigma–Aldrich. Bentonite was procured from Riedel-de Haën while NaOH pellets, concentrated HCl (37% fuming), and ICP multi-element standard solution were from Merck Germany. Analytical grade of $Cu(NO_3)_2{\cdot}2.5H_2O$ was procured from Riedel-de Haën.

2.2. Instrumentation

An ICP-OES Perkin Elmer DV2000 series was used for the quantitative analysis of Cu(II). A Channel Precision Oven model DV452 220 V was used for drying CHB. A peristaltic pump, Masterflex CZ 77120-70, was utilized in the column study. The surface morphology of CHB was analyzed using a scanning electron microscope (SEM, Hitashi S-4800). The surface area and average pore size were determined using the Brunauer, Emmett, and Teller (BET) multipoint technique using N_2 adsorption at 77 K. The thermogravimetric curves of chitosan, bentonite and CHB were obtained using a Perkin Elmer Pyris diamond thermomechanical analyzer with a heating rate at 10 °C per minute in the temperature range of 30–800 °C.

2.3. Preparation of chitosan immobilized on bentonite (CHB)

Chitosan, with a mass of 5.0 g, was dissolved in 300 mL of 5% (v/v) HCl and the solution was stirred for 2 h at 300 rpm. About 100 g of bentonite was added into the solution and was stirred for another 3 h. Chitosan was precipitated onto bentonite by the dropwise addition of 1N NaOH until neutralization occurs. The adsorbent was washed with deionized water, dried in the oven at 65 °C for 24 h and sieved. Adsorbent with a heterogeneous particle size range of 0.50–0.21 mm were used in the column studies.

2.4. Column set-up

The experiments were conducted using a column made of IWAKI glass code 7740, which is composed mainly of borosilicate glass. The column has an internal diameter of 1.2 cm and length of 55 cm. The column was operated in a down flow mode. A fixed amount of glass beads were placed at the bottom of the column to serve as a support material for CHB. Glass beads were placed on top of the adsorbent bed to control the flow of the inlet solution. The pH of the inlet solution is set to pH 4. Effluent samples were collected at the bottom of the column at different time intervals. The Cu(II) residual concentration was analyzed using ICP-OES.

2.5. Column experiments

2.5.1. Effect of bed depth

The effect of varying the bed height (1.3 cm, 2.3 cm, 4.3 cm) on the column parameters were studied. The flow rate of 0.20 mL/min and initial influent concentration of 500 mg/L were kept constant.

2.5.2. Effect of initial influent concentration

Initial influent concentration of 500 mg/L, 750 mg/L, and 1500 mg/L were used to study the effect of solution concentration on the removal of Cu(II). A bed height of 4.3 cm and a flow rate of 0.20 mL/min are kept constant.

2.5.3. Effect of flow rate

Different flow rates of 0.20 mL/min, 0.40 mL/min, and 0.60 mL/min were used and the effect on the column performance was analyzed. The initial inlet concentration and bed height were maintained at 500 mg/L and 2.3 cm, respectively. The flow rates were selected based on the typical range of groundwater velocity.

2.6. Analysis of column data

The performance of a column study is based on the shape of a breakthrough curve. This is done by plotting the normalized effluent Cu(II) concentration (C_t/C_0) against time (t), where C_t and C_0 is the Cu(II) effluent and inlet concentration (mg/L), respectively. The treated effluent volume, V_e is given by Eq. (1):

$$V_e = Qt_e \tag{1}$$

where Q is the volumetric flow rate (mL/min) and t_e is the time at exhaustion (h). The breakthrough and exhaustion points are set at 10% and 90% of the influent concentration, respectively.

The uptake capacity at breakthrough point (q_b) or the amount of Cu(II) bound to CHB at breakthrough is given by the equation (Tor et al., 2009):

$$q_b = \int_0^{V_b} \frac{C_0 - C_t}{M}\, dV \tag{2}$$

where q_b is the breakthrough capacity (mg/g), C_0 and C_t are the influent and Cu(II) effluent concentration (mg/L), M is the mass of CHB (g), and V_b is the volume of solution passed until breakthrough point (mL).

Table 1
Surface area determination of chitosan, bentonite and CHB adsorbents.

	Chitosan	Bentonite	CHB
BET surface area (m^2/g)	1.05	75.14	28.56
Langmuir surface area (m^2/g)	1.11	77.76	31.58
Micropore area (m^2/g)	0.22	30.69	11.19
Average pore diameter (Å)	200.19	67.84	138.06
Total pore volume (cm^3/g)	0.003	0.088	0.019

The capacity of CHB at the exhaustion point, q_e is given by the equation (Tor et al., 2009):

$$q_e = \int_0^{V_e} \frac{C_0 - C_t}{M}\, dV \tag{3}$$

where q_e is the capacity at exhaustion point (mg/g), and V_e is the volume of Cu(II) solution passed until exhaustion occurs (mL).

The length of the mass transfer zone is computed from the breakthrough curve (Vijayaraghavan, Jegan, Palanivelu, & Velan, 2004):

$$Z_m = Z\left(1 - \frac{t_b}{t_e}\right) \tag{4}$$

where Z_m is the length of the mass transfer zone (cm), Z is the bed height (cm), t_b is the time at breakthrough (h) and t_e is the time at exhaustion (h).

The total amount of Cu(II), m_{total} (g) sent to the column is computed by (Vijayaraghavan et al., 2004):

$$m_{total} = \frac{C_0 Q t_e}{1000} \tag{5}$$

The total Cu(II) removal is calculated using equation (Vijayaraghavan et al., 2004):

$$\%\ \text{removal} = \frac{m_{ad}}{m_{total}} \times 100 \tag{6}$$

where m_{ad} is the total metal retained by the column (g), which is the area found above the breakthrough curve and is obtained by numerical integration.

3. Results and discussion

3.1. Characterization of CHB

3.1.1. Surface morphology

Fig. 1 illustrates the SEM micrographs of chitosan, bentonite, and CHB, respectively. Fig. 1(a) represents pure chitosan, which displays a membrane-like, smooth and non-porous surface (Kamari & Ngah, 2009). The morphology of bentonite is shown in Fig. 1(b), where a plate-like structure stacked on top of each other was observed. Fig. 1(c) shows the CHB morphology, where an agglomerated and irregular surface structure was observed. CHB grains are coarser in size in comparison to the bentonite particles.

3.1.2. Specific surface area analysis

The surface area characterization of chitosan, bentonite, and CHB are listed in Table 1. The process of immobilizing chitosan onto bentonite resulted to the homogenous dispersion of the chitosan polymer matrix onto the bentonite surface. This gives rise to the superior properties of CHB over chitosan in terms of higher surface area, total pore volume and micropore area. However, these CHB properties are lower in comparison to the bentonite values with the exception of a larger average pore diameter for CHB. These inferior properties of CHB are caused by the intercalation of chitosan in between the silicate layers of bentonite as well as the occurrence of agglomeration due to the bentonite hydroxylated edges interacting with each other (Wang et al., 2005).

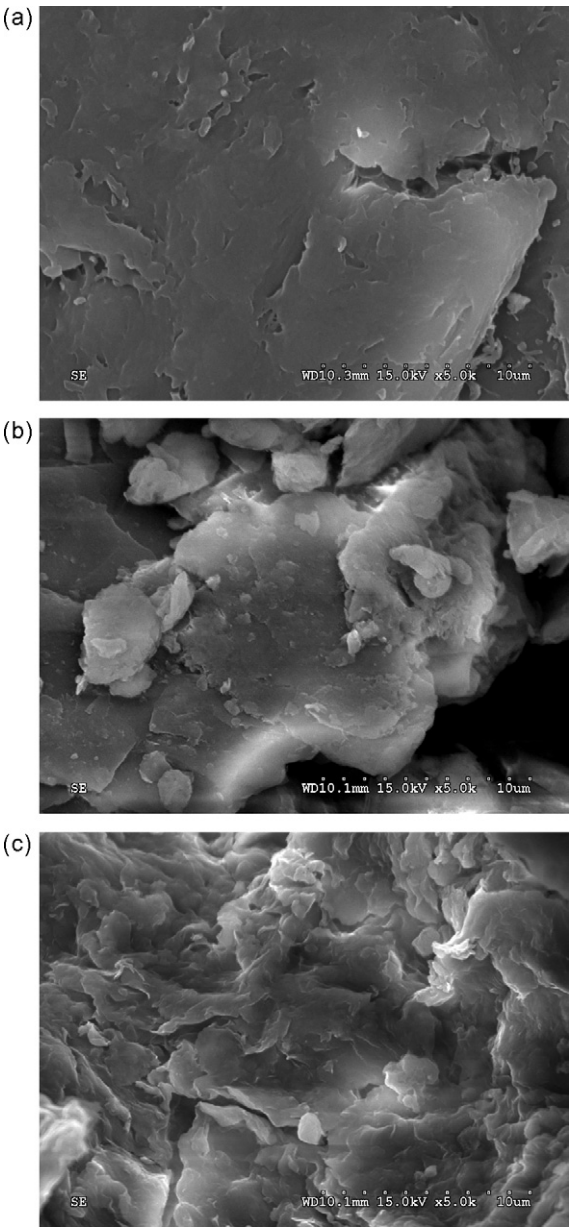

Fig. 1. SEM micrographs of (a) chitosan, (b) bentonite, and (c) CHB.

3.1.3. Thermogravimetric analysis

Fig. 2(a)–(c) illustrates the thermogravimetric curves of bentonite, chitosan, and CHB, respectively. For bentonite, the first major weight loss of 13% is observed near 40–120 °C, which is due to the evaporation of adsorbed water. The second weight loss of 5%, occurred at 500–670 °C, due to loss of structure of the hydroxyl group. Chitosan has 2 major degradation stages: in the range of 40–110 °C and 250–540 °C. The first stage has a weight loss of 8%, caused by the loss of water due to evaporation. The second stage is the maximum weight loss of chitosan (Machado et al., 2009), where it was burnt out completely at 540 °C. Moreover, the TGA curve of CHB is a combination of chitosan's and bentonite's TGA curve in terms of degradation temperatures. A higher weight loss value of 10% is experienced at the second degradation stage, occurring around 250–695 °C. The thermogram of CHB indicates about 3.1% of chitosan was successfully coated onto bentonite.

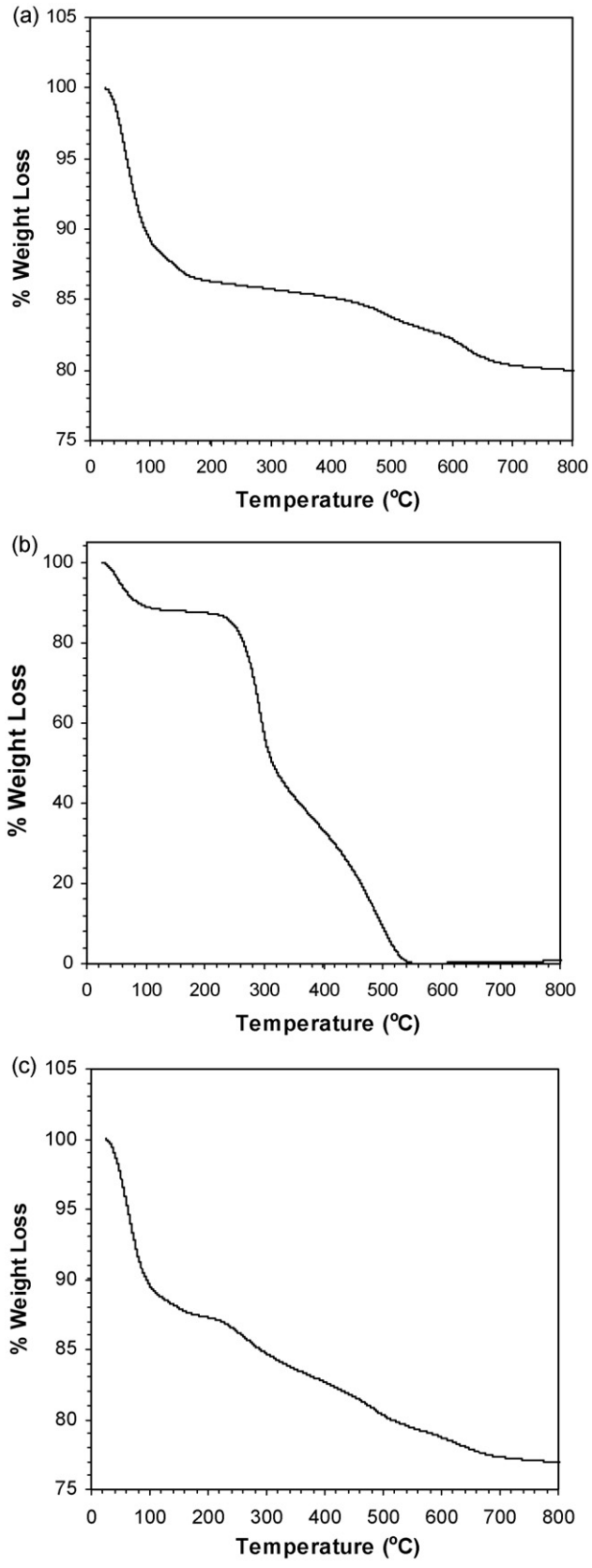

Fig. 2. Thermogravimetric curves of (a) bentonite, (b) chitosan, and (c) CHB.

Table 2
Column parameters of CHB at different bed height, influent concentration, and flow rate.

	V_{eff} (mL)	q_b (mg/g)	q_e (mg/g)	Total Cu(II) removal (%)	Z_m (cm)
Different bed height[a]					
1.3 cm	104.50	13.26	21.22	60.97	0.92
2.3 cm	189.20	14.51	21.73	68.91	0.99
4.3 cm	262.40	14.92	22.27	74.39	0.94
Different influent concentration[b]					
500 mg/L	274.20	16.57	19.55	85.57	1.26
750 mg/L	229.74	18.78	21.06	73.35	1.28
1500 mg/L	149.60	19.31	21.58	68.40	2.30
Different flow rate[c]					
0.20 mL/min	165.40	15.80	26.52	80.20	0.94
0.40 mL/min	208.20	14.40	25.50	61.55	1.10
0.60 mL/min	247.00	13.03	25.01	47.35	1.52

[a] C_0 = 500 mg/L; Q = 0.20 mL/min.
[b] Z = 4.3 cm; Q = 0.20 mL/min.
[c] Z = 2.3 cm; C_0 = 500 mg/L.

3.2. Parameters affecting the column performance

Process parameters like bed height, flow rate, and initial inlet concentration are important in column design. Their effect on the shape of the breakthrough curve and column performance was investigated.

3.2.1. Effect of bed height

Fig. 3(a) illustrates the breakthrough curves obtained at different bed heights (1.3 cm, 2.3 cm, 4.3 cm) with a constant influent concentration of 500 mg/L and flow rate of 0.20 mL/min. As the bed height is decreased from 4.3 cm to 1.3 cm, an increase in the slope from the point of breakthrough up to point of exhaustion is observed and the breakthrough curves become steeper. As the bed height increases, the time of breakthrough and time of exhaustion increases accordingly.

According to Table 2, as the bed height is increased, the volume of effluent treated and total Cu(II) removal (%) increased as well. The total Cu(II) adsorbed at time of breakthrough, q_b and at time of exhaustion, q_e slightly increased with increasing bed height. A higher bed height indicates a larger amount of adsorbent residing in the column, which implies that more binding sites are available as well. At the lowest bed height of 1.3 cm, axial dispersion is the governing mechanism for mass transfer, which means there is no sufficient time for the Cu(II) ions to diffuse into the whole CHB bed, causing a shorter breakthrough time to occur (Qaiser et al., 2009; Taty-Costodes, Fauduet, Porte, & Ho, 2005). The length of the mass transfer zone, Z_m seems unaffected, with only slight changes were observed, as the bed height is increased. This is expected since the length of the mass transfer zone is influenced directly by the variation of flow rate and influent concentration.

3.2.2. Effect of initial inlet concentration

The effect of varying the influent concentration was studied using Cu(II) solution of 500 mg/L, 750 mg/L, and 1500 mg/L while the flow rate of 0.20 mL/min and bed height of 4.3 cm were kept constant. The breakthrough curves at different concentrations are given in Fig. 3(b). Increasing the influent concentration results to a sharper breakthrough curve, as well as a shorter bed service time. The CHB fixed-bed system is saturated more quickly at 1500 mg/L, which decreased the time to reach both the breakthrough and exhaustion point.

As shown in Table 2, varying the initial influent concentration affects the column performance. An increasing influent concentration caused the volume of treated effluent and total Cu(II) removal to decrease. However, the bed adsorption capacity at breakthrough

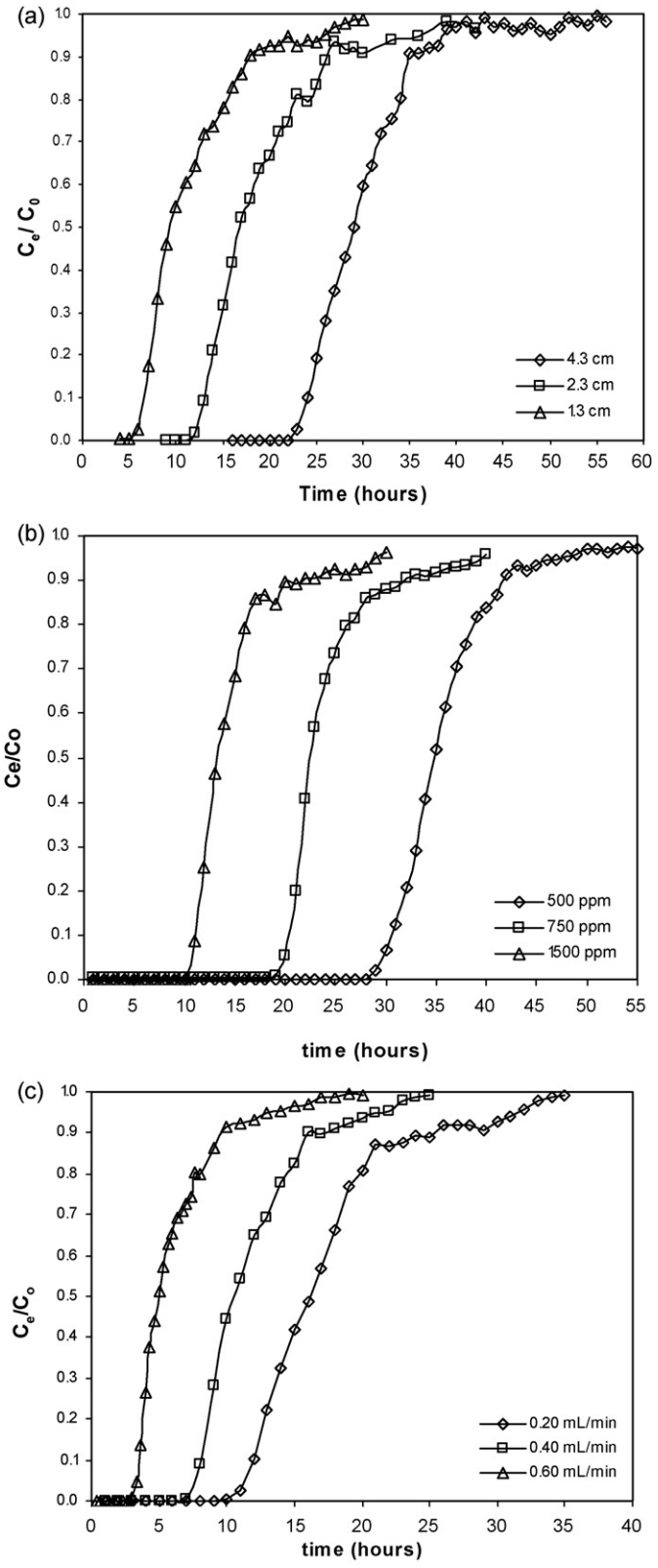

Fig. 3. Breakthrough curves of Cu(II) at (a) different bed heights, (b) different influent concentrations and (c) different flow rates.

and exhaustion were observed to increase from 16.57 mg/g to 19.31 mg/g and from 19.55 mg/g to 21.58 mg/g as the influent concentration was increased from 500 mg/L to 1500 mg/L. A low influent concentration causes the slow transport of Cu(II) ions from the film layer to the surface of the CHB adsorbent due to the lower concentration gradient, which implies a decreased diffusion coefficient and decreased mass transfer driving force (Han et al., 2009; Singh & Pant, 2006). The length of mass transfer zone, Z_m is observed to become smaller as the influent concentration is lowered, which is preferred.

3.2.3. Effect of flow rate

To investigate the effect of varying the flow rates (0.20 mL/min, 0.40 mL/min and 0.60 mL/min), the bed height of 2.3 cm and initial influent concentration of 500 mg/L were held constant. Steep breakthrough curves were observed at higher flow rates, which caused the time of breakthrough and exhaustion to occur earlier. As listed in Table 2, an increase in flow rate from 0.20 mL/min to 0.60 mL/min increases the volume of effluent treated from 165.40 mL to 247.00 mL but decreases the Cu(II) removal efficiency as well as the uptake capacity of Cu(II).

At lowest flow rate of 0.20 mL/min, the highest Cu(II) removal of 80.20% and highest bed adsorption capacity at breakthrough and exhaustion is obtained at 15.80 mg/g and 26.52 mg/g, respectively. A high flow rate results to a weak distribution of Cu(II) ions in the CHB bed resulting in insufficient resident time for the diffusion of Cu(II) ions within the adsorbent bed, where the solution leaves before equilibrium occurs, resulting to a low uptake capacity and removal efficiency (Vijayaraghavan et al., 2004). The diffusion of the Cu(II) ions from the solution to the surface of CHB is made possible by the development of a concentration gradient at the interface. Higher flow rates disturb the film surrounding the CHB particles thereby reducing the adhesion of Cu(II) ions on the CHB surface(Singh & Pant, 2006).

The length of the mass transfer zone, Z_m is observed to increase from 0.94 cm to 1.52 cm with flow rate. A broader mass transfer zone causes the breakthrough and exhaustion to occur earlier.

3.2.4. Comparison of adsorption capacity with other chitosan-based materials

The adsorption capacities (mg Cu(II) adsorbed per g of chitosan) of chitosan-based adsorbents collected from literature are listed in Table 3, in which the results from this study was included for comparison. The present column study gave the highest adsorption capacity, 14.92 mg Cu(II)/g CHB or 480.97 mg Cu(II)/g chitosan, when compared to other chitosan-based adsorbents. The q_e of chitosan from CHB composite has a higher value than the capacity of chemically modified chitosan like H_2SO_4 modified chitosan and glutaraldehyde cross-linked epoxymated chitosan. Providing a support material for chitosan results to an increase in its adsorption capacity because its binding sites become more accessible for Cu(II) ions. This indicates the potential of CHB to be used as a possible reactive material for PRBs.

3.3. Breakthrough curve models

3.3.1. Bed depth service time (BDST) model

The BDST equation was initially derived from the model described by Bohart–Adams, but was modified by Hutchins. It is one of the most widely used models that describe the heavy metal adsorption using a packed bed system. It assumes that the rate of adsorption is governed by the surface reaction between the adsorbate and the unused capacity of the adsorbent. It does not take into account the intraparticle mass transfer resistance as well as the external film resistance where the adsorbate is directly adsorbed onto the surface of the adsorbent (Qaiser et al., 2009). The BDST

Table 3
Comparative adsorption capacity of different chitosan-based adsorbents for Cu(II) removal.

Adsorbent	Type of study	Adsorption capacity (mg Cu(II)/g chitosan)	Reference
CHB	Column	480.97	This study
Chitosan-coated sand	Batch	289.35	Wan et al. (2010)
Hydrolyzed polyacrylamide–chitosan complex beads	Batch	49.07	Cao, Tan, Che, and Xin (2010)
H_2SO_4 modified chitosan	Batch	270.00	Kamari and Ngah (2009)
Glutaraldehyde cross-linked epoxymated chitosan	Batch	199.04	Anirudhan and Rijith (2009)
Chitosan-coated PVC beads	Batch	175.80	Popuri et al. (2009)
Chitosan-coated perlite	Batch	196.10	Kalyani, Priya, Rao, and Krishnaiah (2005)

equation shows a linear relationship between the bed height and breakthrough time, often called service time of the bed (Kumar & Chakraborty, 2009). It is given by the equation:

$$t_s = \frac{N_0 Z}{C_0 U_0} - \frac{1}{k_{ads} C_0} \ln\left(\frac{C_0}{C_b} - 1\right) \quad (7)$$

where t_s is the service time (h), C_0 and C_b are the influent concentration and the breakthrough effluent concentration (mg/L), Z is the bed height (cm), U_0 is the linear flow rate (cm/h), k_{ads} is the adsorption rate constant that describes the mass transfer from the liquid phase to the solid phase (L/(mg h)), and N_0 is the dynamic bed capacity (g/L).

The critical bed depth, Z_0 is calculated by setting $t = 0$ and $C_t = C_b$. It is given by the equation:

$$Z_0 = \frac{U_0}{k_{ads} N_0} \ln\left(\frac{C_0}{C_b} - 1\right) \quad (8)$$

The BDST equation was applied on the column experimental data obtained from varying the bed height from 1.3 cm to 4.3 cm while the flow rate of 0.20 mL/min and initial concentration of 500 mg/L were kept constant. The dynamic bed capacity, N_0 and adsorption rate constant, k_{ads} were computed to be 29.94 g/L, and 0.000857 L/(mg h), respectively. A larger value for k_{ads} implies that even at lower bed heights, breakthrough will occur at a later time whereas a smaller k_{ads} value needs a higher bed height to avoid breakthrough (Vijayaraghavan et al., 2004). The critical bed depth, Z_0 was determined to be 0.9187 cm. This value is the minimum theoretical bed height of the CHB adsorbent that is sufficient such that the effluent concentration at $t = 0$ will not exceed the breakthrough concentration, C_b. This also refers to the theoretical length of the mass transfer zone. Comparing $Z_0 = 0.9187$ cm to the Z_m values (0.92 cm, 0.99 cm, 0.94 cm for bed height of 1.3 cm, 2.3 cm, and 4.3 cm, respectively) obtained from Table 2, Z_0 and Z_m values are very similar regardless of the difference in bed heights.

The BDST model could be used to predict breakthrough times at a different flow rate. An experiment conducted using Q_1 as flow rate would give the BDST equation:

$$t_s = a_1 Z + b_1 \quad (9)$$

Using a new flow rate of Q_2, a new BDST equation is given by:

$$t_s = a_2 Z + b_1 \quad (10)$$

and

$$a_2 = a_1 \left(\frac{Q_1}{Q_2}\right) \quad (11)$$

where a_1 and a_2 are the slopes of the BDST equations at flow rate of Q_1 and Q_2, respectively. The value of the y-intercept used is the same since it is independent of the flow rate in the BDST equation (Kumar & Chakraborty, 2009).

BDST model could be used to design a column system in treating a new influent concentration, C_2 by using the data collected from the previous experiment with a different influent concentration. The experiment conducted, which utilized the influent concentration C_1 is given by:

$$t = r_1 X + s_1 \quad (12)$$

The equation using a new flow rate of Q_2 is given by:

$$t = r_2 X + s_2 \quad (13)$$

The new slope and intercept are computed using:

$$r_2 = r_1 \left(\frac{C_1}{C_2}\right) \quad (14)$$

and

$$s_2 = s_1 \frac{C_1}{C_2} \left\{\frac{\ln[(C_2/C_F) - 1]}{\ln[(C_1/C_b) - 1]}\right\} \quad (15)$$

where r_1 and r_2 are the slopes, s_1 and s_2 are the y-intercepts, and C_F and C_b are the effluent concentrations at influent concentrations C_1 and C_2, respectively.

Using Eqs. (9)–(15), the theoretical breakthrough times were predicted at different flow rate and influent concentration and are listed in Table 4. The theoretical breakthrough times at different flow rates are in good agreement with its experimental values whereas the predicted breakthrough times at different influent concentrations slightly deviated from the experimental values obtained.

3.3.2. Thomas model

Thomas model is one of the most widely used in describing the column performance and prediction of breakthrough curves. The model follows the Langmuir kinetics of adsorption–desorption. It assumes negligible axial dispersion in the column adsorption since the rate driving force obeys the second-order reversible reaction kinetics (Suksabye, Thiravetyan, & Nakbanpote, 2008). It is given by the equation below (Aksu & Gonen, 2004):

$$\frac{C_0}{C_t} = \frac{1}{1 + \exp[(k_{Th}/Q)(Q_0 M - C_0 V_t)]} \quad (16)$$

where Q is the flow rate (mg/L), M is the mass of adsorbent (g), V_t is the volume of effluent treated (mL), Q_0 is the maximum solid phase concentration of Cu(II) per weight of CHB (mg/g), and k_{Th} is the Thomas rate constant (mL/(mg min)).

The linearized form of the Thomas model is a follows:

$$\ln\left(\frac{C_t}{C_0} - 1\right) = \frac{k_{Th} Q_0 M}{Q} - \frac{k_{Th} C_0}{Q} V_t \quad (17)$$

where plotting $\ln[(C_t/C_0) - 1]$ against t will determine the Thomas constants Q_0 and k_{Th}.

Table 5 lists the calculated Thomas constants from the experimental column data when the flow rate and initial influent concentration were varied. The correlation coefficient values ranged from 0.9054 to 0.9758, indicate a good agreement between the experimental data and the column data generated using the Thomas model. This is further validated by Fig. 4, where it shows the predicted breakthrough curves and experimental points at different influent concentrations and flow rates. It clearly indicates a

Table 4
Comparison of the theoretical breakthrough times derived from the BDST approach with the experimental breakthrough times under various operating conditions.

Q[a] (mL/min)	Breakthrough time (h)		C_0[b] (mg/L)	Breakthrough time (h)	
	Theoretical	Experimental		Theoretical	Experimental
0.20	12.79	12.00	500	27.07	30.00
0.40	6.30	8.00	750	18.12	21.00
0.60	4.13	3.80	1500	9.21	11.00

[a] Operating conditions: Z = 2.3 cm; C_0 = 500 mg/L.
[b] Operating conditions: Z = 4.3 cm; Q = 0.20 mL/min.

Table 5
Thomas model parameters at different flow rate and influent concentration for Cu(II) adsorption onto CHB.

Z (cm)	Q (mL/min)	C_0 (mg/L)	Q_0 (mg/g)	k_{Th} (mL/(mg min))	R^2
2.3	0.20	500	35.04	0.0010	0.9690
2.3	0.40	500	34.77	0.0011	0.9087
2.3	0.60	500	33.54	0.0014	0.9380
4.3	0.20	500	32.93	0.0008	0.9758
4.3	0.20	750	33.79	0.0004	0.9402
4.3	0.20	1500	40.38	0.0002	0.9054

good agreement between the experimental points and the simulated curves predicted by the Thomas model.

The values of Q_0 increased while k_{Th} decreased with increasing initial concentration. The opposite trend is observed for the column data obtained in varying the flow rate. The rate constant, k_{Th} is observed to increase with increase in flow rate, which is caused by a decrease in the mass transport resistance. The thickness of the liquid film on the CHB adsorbent surface has a direct effect on the mass transfer resistance (Tor et al., 2009). Higher flow rates enhances the mass transfer of Cu(II) ions from the liquid film to the adsorbent surface, leading to earlier saturation of the adsorbent bed. On the other hand, Q_0, is observed to decrease with increase in flow rate since there is no sufficient time for Cu(II) ions to diffuse into the CHB bed.

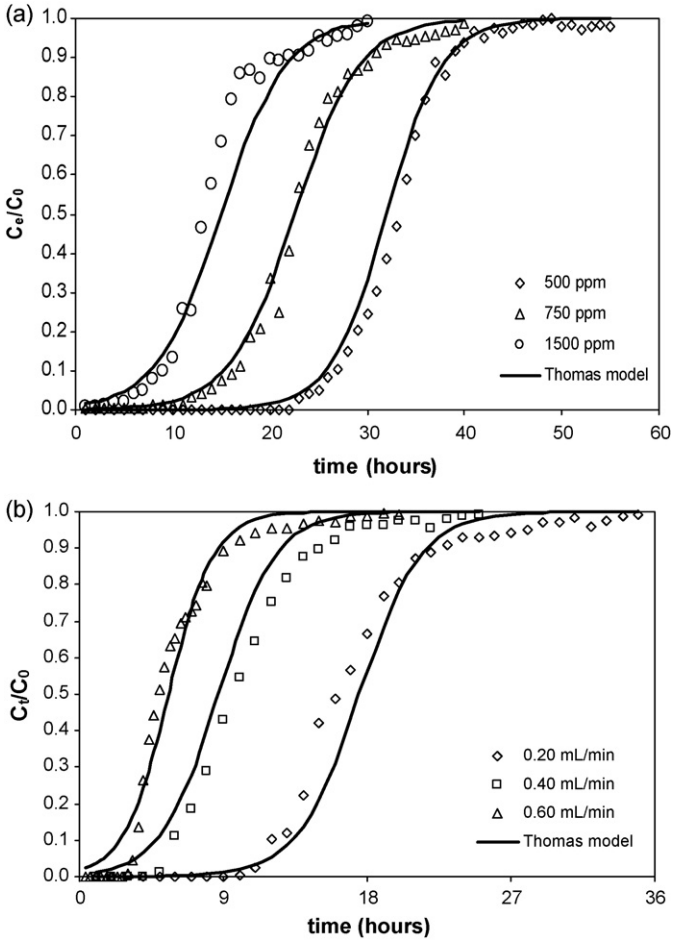

Fig. 4. The experimental and predicted breakthrough curves of Cu(II) at (a) different influent concentrations and (b) different flow rates using the Thomas model.

4. Conclusions

The removal of Cu(II) in a packed bed system using CHB as an adsorbent is an effective and feasible method. The shape of the breakthrough curve and the Cu(II) uptake capacity of the CHB bed is strongly dependent on the bed height, flow rate, and influent concentration. A longer breakthrough and exhaustion time occurred at a higher bed height, a lower flow rate, and lower influent concentration. At the optimum condition, the adsorption capacity value is 14.92 mg/g CHB with time of breakthrough and exhaustion at 24 h and 35 h, respectively.

The prediction of breakthrough curves and the determination of the kinetic column parameters were obtained by using the BDST model and Thomas model. The Thomas model provided a good correlation in the prediction of the breakthrough curves due to its acceptable R^2 values (0.9054–0.9758) as well as a good agreement observed between the simulated breakthrough curves and the experimental data points. The BDST model equation was used in predicting the theoretical breakthrough times at different flow rates and influent concentrations. The predicted values at different flow rates were in good agreement with the experimental values whereas a slight deviation with the experimental and theoretical values was observed at different influent concentrations.

In this study, CHB has been found to have the highest adsorption capacity in comparison to other chitosan-based derivatives. Finally, this information is essential in the practical designs of permeable reactive barrier (PRB) applied to the recovery of heavy metals from groundwater.

Acknowledgements

The authors would like to acknowledge the Philippine ERDT scholarship and Taiwan National Science Council (NSC 97-2221-E-041-016) for their financial support.

Appendix A.

C_0	influent concentration (mg/L)
C_b	concentration at breakthrough point (mg/L)
C_t	effluent concentration at any time t (mg/L)
k_{ads}	BDST adsorption rate constant (L/(mg h))
k_{Th}	Thomas rate constant (mL/(mg min))
m_{ad}	amount of metal retained by the column (g)
m_{total}	total amount of metal sent to the column (g)
M	mass of the adsorbent (g)
N_0	dynamic bed capacity (g/L)

q_b uptake capacity at breakthrough point (mg/g)
q_e uptake capacity at exhaustion point (mg/g)
Q volumetric flow rate (mL/min)
Q_0 maximum solid phase concentration of Cu(II) per weight of CHB (mg/g)
t_b time at breakthrough (h)
t_e time at exhaustion (h)
t_s bed service time (h)
U_0 linear flow rate (cm/h)
V_b volume of solution passed until breakthrough point (mL)
V_e volume of solution passed until exhaustion point (mL)
Z_m length of the mass transfer zone (cm)
Z_0 BDST critical bed depth (cm)
Z bed height (cm)

References

Aksu, Z., & Gonen, F. (2004). Biosorption of phenol by immobilized activated sludge in a continuous packed bed: Prediction of breakthrough curves. *Process Biochemistry*, *39*, 599–613.

Anirudhan, T. S., & Rijith, S. (2009). Glutaraldehyde cross-linked epoxyaminated chitosan as an adsorbent for the removal and recovery of copper(II) from aqueous media. *Colloids Surfaces A: Physicochemical and Engineering Aspects*, *351*, 52–59.

Bhattacharyya, K. G., & Gupta, S. S. (2006). Kaolinite, montmorillonite, and their modified derivatives as adsorbents for removal of Cu(II) from aqueous solution. *Separation and Purification Technology*, *50*, 388–397.

Cao, J., Tan, Y., Che, Y., & Xin, H. (2010). Novel complex beads composed of hydrolyzed polyacrylamide and chitosan: An affective adsorbent for the removal of heavy metal from aqueous solution. *Bioresource Technology*, *101*, 2558–2561.

Chang, M. Y., & Juang, R. S. (2004). Adsorption of tannic acid, humic acid, and dyes from water using the composite of chitosan and activated clay. *Journal of Colloid and Interface Science*, *278*, 18–25.

Han, R, Zou, L., Zhao, X., Xu, Y., Xu, F., Li, Y., et al. (2009). Characterization and properties of iron oxide-coated zeolite as adsorbent for removal of copper(II) from solution in fixed bed column. *Chemical Engineering Journal*, *149*, 123–131.

Kalyani, S., Priya, J. A., Rao, P. S., & Krishnaiah, A. (2005). Removal of copper and nickel from aqueous solutions using chitosan coated on perlite as biosorbent. *Separation Science and Technology*, *40*, 1483–1495.

Kamari, A., & Ngah, W. S. (2009). Isotherm, kinetic, and thermodynamic studies of lead and copper uptake of H_2SO_4 modified chitosan. *Colloids and Surfaces B: Biointerfaces*, *73*, 257–266.

Kumar, P. A., & Chakraborty, S. (2009). Fixed-bed column study for hexavalent chromium removal and recovery by short-chain polyaniline synthesized on jute fiber. *Journal of Hazardous Materials*, *162*, 1086–1098.

Li, S. Z., & Wu, P. X. (2010). Characterization of sodium dodecyl sulfate modified iron pillared montmorillonite and its application for the removal of aqueous Cu(II) and Co(II). *Journal of Hazardous Materials*, *173*, 62–70.

Machado, M. O., Lopes, E., Sousa, K. S., & Airoldi, C. (2009). The effectiveness of the protected amino group on crosslinked chitosans for copper removal and the thermodynamics of interaction at the solid/liquid interface. *Carbohydrate Polymers*, *77*, 760–766.

Popuri, S. R., Vijaya, Y., Boddu, V. M., & Abburi, K. (2009). Adsorptive removal of copper and nickel ions from water using chitosan-coated PVC beads. *Bioresource Technology*, *100*, 194–199.

Qaiser, S., Saleemi, A. R., & Umar, M. (2009). Biosorption of lead from aqueous solution by *Ficus religiosa* leaves: Batch and column study. *Journal of Hazardous Materials*, *166*, 998–1005.

Singh, T. S., & Pant, K. K. (2006). Experimental and modeling studies on fixed bed adsorption of As(II) ions from aqueous solution. *Separation and Purification Technology*, *48*, 288–296.

Suksabye, P., Thiravetyan, P., & Nakbanpote, W. (2008). Column study of chromium(VI) adsorption from electroplating industry by coconut coir pith. *Journal of Hazardous Materials*, *160*, 56–62.

Taty-Costodes, V. C., Fauduet, H., Porte, C., & Ho, Y. S. (2005). Removal of lead (II) ions from synthetic and real effluents using immobilized *Pinus sylvestris* sawdust: Adsorption on a fixed bed column. *Journal of Hazardous Materials*, *B123*, 135–144.

Tor, A., Danaoglu, N., Arslan, G., & Cengeloglu, Y. (2009). Removal of fluoride from water by using granular red mud: Batch and column studies. *Journal of Hazardous Materials*, *164*, 271–278.

Varma, A. J., Deshpande, S. V., & Kennedy, J. F. (2004). Metal complexation by chitosan and its derivatives: A review. *Carbohydrate Polymers*, *55*, 77–93.

Vijayaraghavan, K., Jegan, J., Palanivelu, K., & Velan, M. (2004). Removal of nickel (II) ions from aqueous solution using crab shell particles in a packed bed up-flow column. *Journal of Hazardous Materials*, *B113*, 223–230.

Wan, M. W., Kan, C. C., Rogel, B. D., & Dalida, M. L. (2010). Adsorption of copper(II) and lead(II) ions from aqueous solution on chitosan-coated sand. *Carbohydrate Polymers*, *80*, 891–899.

Wang, L., & Wang, A. (2008). Adsorption behaviors of Congo red on the N O-carboxymethyl-chitosan/montmorillonite nanocomposite. *Chemical Engineering Journal*, *143*, 43–50.

Wang, S. F., Shen, L., Tong, Y. J., Chen, L., Phang, I. Y., Lim, P. Q., et al. (2005). Biopolymer chitosan/montmorillonite nanocomposites: Preparation and characterization. *Polymer Degradation and Stability*, *90*, 123–131.

Wu, P., Wu, W., Li, S., Xing, N., Zhu, N., Li, P., et al. (2009). Removal of Cd^{2+} 452 from aqueous solution by adsorption using Fe-montmorillonite. *Journal of Hazardous Materials*, *169*, 824–830.